

VARIABLE STARS IN THE VVV GLOBULAR CLUSTERS. I. 2MASS-GC02 AND TERZAN 10

JAVIER ALONSO-GARCÍA^{1,2}, ISTVÁN DÉKÁNY^{2,1}, MÁRCIO CATELAN^{1,2}, RODRIGO CONTRERAS RAMOS^{1,2}, FELIPE GRAN^{1,2}, PÍA AMIGO^{3,2}, PAUL LEYTON^{1,2}, AND DANTE MINNITI^{4,1,2,5}

Draft version June 20, 2021

ABSTRACT

The VISTA Variables in the Vía Láctea (VVV) ESO Public Survey is opening a new window to study the inner Galactic globular clusters using their variable stars. These globular clusters have been neglected in the past due to the difficulties caused by the presence of an elevated extinction and high field stellar densities in their lines of sight. However, the discovery and study of any present variables in these clusters, especially RR Lyrae stars, can help to greatly improve the accuracy of their physical parameters. It can also help to shed some light on the interrogations brought by the intriguing Oosterhoff dichotomy in the Galactic globular cluster system. In a series of papers we plan to explore the variable stars in the globular clusters falling inside the field of the VVV survey. In this first paper we search and study the variables present in two highly-reddened, moderately metal-poor, faint, inner Galactic globular clusters: 2MASS-GC02 and Terzan 10. We report the discovery of sizable populations of RR Lyrae stars in both globular clusters. We use near-infrared period-luminosity relations to determine the color excess of each RR Lyrae star, from which we obtain both accurate distances to the globular clusters and the ratios of the selective to total extinction in their directions. We find the extinction towards both clusters to be elevated, non-standard, and highly differential. We also find both clusters to be closer to the Galactic center than previously thought, with Terzan 10 being on the far side of the Galactic bulge. Finally, we discuss their Oosterhoff properties, and conclude that both clusters stand out from the dichotomy followed by most Galactic globular clusters.

Subject headings: globular clusters: general — globular clusters: individual (2MASS-GC02, Terzan 10)
— stars: variables: general — stars: variables: RR Lyrae

1. INTRODUCTION

Observations of most of the globular clusters (GCs) located in the Galactic bulge region are severely affected by the effects of reddening, both absolute and differential, and by high densities of field stars (Valenti et al. 2007; Alonso-García et al. 2012). This highly complicates the analysis and interpretation of their color-magnitude diagrams (CMDs), and the accuracy of the physical parameters obtained therefrom. This is especially dramatic in the case of low-surface brightness, inner-Galactic GCs, which complicates even their very detection (e.g., Hurt et al. 2000; Minniti et al. 2011; Moni Bidin et al. 2011).

The analysis of any variable star content, especially RR Lyrae, in the inner Galactic GCs is invaluable for better determining their physical parameters. RR Lyrae are bright radial pulsators, present in considerable numbers in most of the old Galactic GCs (Clement et al. 2001). They have been shown to follow tight period-luminosity relations in the near-infrared wavebands, especially in the *K*-band (e.g., Longmore et al. 1986, 1990; Catelan et al. 2004), that can be used as a powerful tool for distance determinations. But a systematic census and measure-

ment of accurate near-infrared light curves of RR Lyrae variables in the inner Galactic GCs have been pending until now. Fortunately, the *VISTA Variables in the Vía Láctea* (VVV) ESO Public Survey provides a headway in improving this situation. VVV is a multi-epoch, near-infrared survey that covers most of the bulge region of our Galaxy, along with a region of the Southern disk with high star formation, using ESO's 4-m VISTA Telescope in Chile (Minniti et al. 2010; Saito et al. 2011; Catelan et al. 2011). Numerous inner Galactic globular clusters, 2MASS-GC02 and Terzan 10 among them, fall inside the area covered by the VVV survey. This allows us to detect the variable stars of these clusters, derive their periods and mean magnitudes, analyze their light curves, determine their variability types, and employ them, especially any discovered fundamental-mode RR Lyrae pulsators, for a more accurate determination of the physical parameters of their host GCs.

A particular characteristic of the Galactic GCs is the Oosterhoff dichotomy (Oosterhoff 1939; Catelan 2009a; Smith et al. 2011). The GCs in the Milky Way are clumped into two main groups: Oosterhoff I contains fundamental-mode RR Lyrae (RRab) with shorter periods ($\langle P_{\text{ab}} \rangle \sim 0.55$ days), and Oosterhoff II have RRab's with longer periods ($\langle P_{\text{ab}} \rangle \sim 0.64$ days), leaving an almost empty gap, the so-called Oosterhoff gap, at $\langle P_{\text{ab}} \rangle \sim 0.60 \pm 0.02$ days. This dichotomy seems not to be present in other nearby extragalactic systems, which tend to be preferentially Oosterhoff-intermediate. The interpretation of the Oosterhoff dichotomy in terms of the history of Galactic assembly has been extensively debated. Yoon & Lee (2002) theorized that the dichotomy is a re-

¹ Instituto de Astrofísica, Facultad de Física, Pontificia Universidad Católica de Chile, Av. Vicuña Mackenna 4860, 782-0436 Macul, Santiago, Chile

² Millennium Institute of Astrophysics, Av. Vicuña Mackenna 4860, 782-0436 Macul, Santiago, Chile.

³ Instituto de Física y Astronomía, Universidad de Valparaíso, Av. Gran Bretaña 1111, Playa Ancha, Casilla 5030, Chile

⁴ Departamento de Ciencias Físicas, Universidad Andrés Bello, República 220, Santiago, Chile

⁵ Vatican Observatory, Vatican City State V-00120, Italy.

sult of the decoupled age and metallicity distributions of the Galactic GC system, in which the most metal-poor GCs are younger than the oldest "genuine" Galactic ones and were accreted from satellites. However, Catelan (2009a) argued that age determinations from detailed case studies of halo Galactic GCs have not provided enough evidence for this scenario. In any case, the Oosterhoff dichotomy implies that the oldest components of the Milky Way cannot have formed by pure accretion of the early counterparts of its present-day dwarf galaxy satellites (Catelan 2009a,b). It is important to add that our current sample of Galactic GCs with firm knowledge about their Oosterhoff properties is still incomplete. In particular, bulge GCs are largely unexplored in this respect, mostly due to the lack of time series observations. Among the few exceptions with known Oosterhoff properties, NGC 6441 and NGC 6388 stand out from the Oosterhoff types of both Galactic and extragalactic GCs, with $\langle P_{\text{ab}} \rangle$ too long for their metallicities, forming the so-called Oosterhoff III group (Pritzl et al. 2000, 2001, 2002, 2003; Corwin et al. 2006). This property has been attributed to the presence of a helium-enhanced population of stars in these clusters (Caloi & D'Antona 2007; Yoon et al. 2008), causing the RR Lyrae stars of this population to have longer periods, although it remains unclear why seemingly all the RR Lyrae stars are helium-enhanced in these two clusters. By observing the yet unknown Oosterhoff properties of the bulge GCs, we expect to gain new insights into the formation and evolution of these clusters, and of the central components of the Milky Way itself.

In a series of papers, we will explore the near-infrared time-domain of the inner Galactic GCs in the framework the VVV survey, characterize their variable star content, and derive the GCs' physical parameters therefrom. In the present paper, the first of this series, we have chosen to study two metal-intermediate, low-surface brightness GCs that show some of the highest reddening in the VVV sample of GCs, 2MASS-GC02 and Terzan 10.

2. OBSERVATIONS AND DATA REDUCTION

Our observations are part of the VVV survey, that is being conducted since early 2010 with the 4.1m VISTA Telescope in Cerro Paranal Observatory, in Chile. The VIRCAM camera on the telescope consists of 16 detectors, each of them providing near-infrared images of $11'6 \times 11'6$ with a pixel size of $0''.34$. We used the stacks of 2 slightly dithered ($\approx 20''$ in each direction) individual exposures of the VVV fields that contain our target GCs, 2MASS-GC02 and Terzan 10. The main characteristics of these GCs are listed in Table 1. Since the field provided by the stacked images is sparsely populated, with significant gaps between the chips, a mosaic pattern is needed for a contiguous coverage of every field observed in the VVV (Minniti et al. 2010; Saito et al. 2012), and every region covered in our study is observed a minimum of 2 times and a maximum of 6 times per epoch. The individual images were reduced, astrometrized and stacked by the Cambridge Astronomy Survey Unit (CASU) using the VISTA Data Flow System (VDFS) pipeline (Emerson et al. 2004; Irwin et al. 2004; Hambly et al. 2004). Although so-called *tiles*, i.e. mosaic images with contiguous coverage of the whole detector area at every field, combined from 6 offset stacked images at each epoch, are

also provided by CASU, we decided to work with the individual stacked images. This way we avoid problems in the photometry extraction related with combining offset images, which have different geometrical distortions for a given sky region producing highly space-varying and difficult-to-model point-spread functions (PSF) for the detected objects, and problems related with combining different chips, with significant differences in their dynamic range in some cases. A set of 43 epochs in K_s for 2MASS-GC02 and a set of 101 epochs in K_s for Terzan 10 were available at the time of our variability study. We also used the single-epoch Z , Y , J , and H images for every cluster to build the CMDs and calculate the stellar extinctions, as we show in the following sections. Most epochs in K_s correspond to different nights, and the seeing in most of them was very good, between $0.6''$ and $1.2''$. A summary of the observations is provided in Table 2.

PSF photometry was carried out on the individual processed stacked images using an updated version of DoPHOT (Schechter et al. 1993; Alonso-García et al. 2012). CASU also provides catalogs of aperture photometry, and we used them to calibrate our PSF photometry into the VISTA system. We chose to perform the PSF photometry out to a distance of $10'$ from the cluster center, well beyond both GCs' tidal radii (see Table 1), to also explore a significant region around the GCs, looking for extra-tidal variables and comparing cluster vs. field ratios of variables in the surroundings of the GCs. Certainly this is one of the advantages provided by the big area surveyed by VVV. Photometry for the same object in the different available images was cross-correlated using the STILTS package (Taylor 2006). The generated light curves were next analyzed for variability.

3. VARIABILITY ANALYSIS

We started our variability analysis by performing iterative 10σ and 5σ threshold rejections in the light curves, in order to omit outliers that could heavily bias our analyses. Then, we performed a first selection of candidate variable stars by taking advantage of the correlated sampling of the time-series, i.e., multiple (2–6) points at each epoch, resulting from the subsequent exposures with slightly offset pointings necessary to get a contiguous coverage of the field, as described in Section 2. These batches of successive exposures are always taken within a few minutes of time, which is by orders of magnitude shorter than both the time between two separate batches, and the typical time-scale of stellar variability of our interest. Therefore, the fluxes measured within such a sequence can well be considered to sample the light curve at the same epoch, thus the differential flux within them will be dominated by noise. Likewise, the deviations of the fluxes measured from the average brightness, for instance, will be expected to be well correlated within such batches in case of intrinsically variable stars, and rather uncorrelated otherwise. A well-known descriptive statistic that was specifically designed to measure this kind of correlations in astronomical time-series with such sampling is the so-called Stetson's index (Welch & Stetson 1993; Stetson 1996). We employed the generalized version of this statistic (Stetson 1996, Eq. 1) for pre-selecting a first set of variable star candidates, by requiring the value of the Stetson index to be higher than

a pre-determined critical threshold. The latter was set as the value of the index at the 0.1% significance level corresponding to pure Gaussian noise, and was derived from Monte Carlo simulations for various different numbers of observational epochs. This procedure resulted in our broad *first selection* of candidate variable stars, including $\sim 10^4$ light curves in the areas surrounding both clusters.

Candidates pre-selected by their Stetson index were subjected to frequency analysis. First, we binned the light curves in order to simplify the assessment of spectral significance, i.e. we computed the weighted averages of the magnitudes in each batch of stacked images, resulting in light curves with one point per epoch. Then we computed both the Generalized Lomb-Scargle periodogram (Zechmeister & Kürster 2009, GLS) and the phase dispersion spectrum (Stellingwerf 1978, PDM) of each light curve, and determined the primary frequency components from both methods in the $[0 - 10] \text{ d}^{-1}$ frequency range, using a spectral oversampling factor of 10. Significance levels of these components were estimated analytically. We selected the light curves that showed periodic signals detected with better than 0.1% significance by both methods (not requiring the frequencies to coincide). We rejected signals with close to integer d^{-1} frequencies in order to exclude false alarms triggered by typical systematics of ground-based observations (see, e.g., Kovács et al. 2005). However, we considered light curves showing low-frequency spectral excess with a total amplitude of $\geq 0.1 \text{ mag}$, which could be indicative of periodic signals with periods longer than the time span of our observations, or aperiodic variations such as transients. Our procedure resulted in our narrow *second selection* of ~ 2000 and ~ 5000 variable star candidates in the case of 2MASS-GC02 and Ter 10, respectively.

In the next step of our analysis, we performed a combined visual inspection of both the phase diagrams and the images of each and every object in the *second selection*, and rejected those which did not meet some basic phenomenological criteria. Most rejected light curves had obvious signs of temporal saturation and/or blending and showed false signals originating from these effects. In addition, a large number of sources turned out to be fake variables, with periodic signals emanating from the temporally contaminating flux from the rotating diffraction spikes of nearby saturated stars (due to the altazimuthal configuration of VISTA). As a result of this procedure, we narrowed down our selection to 102 and 160 variables in the field of 2MASS-GC02 and Ter 10, respectively.

As a final step in our time-series analysis, we performed an iterative refinement procedure on the *unbinned* light curves. We performed a non-linear Fourier fit using the frequencies from the GLS/PDM analyses as initial values, visually optimizing the number of Fourier orders for each object. In cases where the frequencies from the two methods had a significant discrepancy, we adopted the one that produced the smaller χ^2 . We then performed a threshold rejection around the fit, and refitted the light curve until the procedure converged in a final solution. The apparent K_s -band equilibrium brightnesses of the stars were estimated by the intensity-averaged magnitudes of the stars, computed from the Fourier fits to the light curves. The total amplitudes of the light curves

were computed from the Fourier fits.

We tried to assign a variability type to the discovered variables, but this task proved to be non-trivial. Most variable stars are more difficult to be classified in the near-infrared bands, especially in K_s , because their light curves contain less features than in the optical (e.g., fundamental-mode RR Lyrae show smaller amplitudes and more sinusoidal light curves in the near-infrared than in the optical), and there is a general absence of near-infrared template light curves, compared to the situation in the optical. Within the VVV collaboration we are trying to solve this shortcoming with the VVV Templates Project (Angeloni et al. 2014), which will eventually lead to automated classification of all VVV light curves (Catelan et al. 2013). Since we are still developing the algorithms for such an automated classification, for the present study we adopted an "eyeball" classification, providing a type only for those variables that had well-measured light curves and could be securely classified based on their periods and characteristic light curve features. Fundamental-mode RR Lyrae stars, Cepheids, eclipsing binaries (mostly of Algol-type), and long-period variables (LPVs), are found among the stars that we believe could be reliably classified in this way.

4. 2MASS-GC02

2MASS-GC02 is an inner Galactic GC, only recently discovered by Hurt et al. (2000) serendipitously during a spot check of 2MASS images for quality assurance review. Its elevated extinction made it invisible in earlier optical observations. Since its discovery, there have been a few photometric studies trying to determine its physical parameters (Ivanov et al. 2000; Borissova et al. 2002, 2007), with a range of values proposed for extinction and distances, depending on various metallicity and chemical enrichment scenarios. Ivanov et al. (2000) quoted values $(m - M)_0 = 12.98$ and $E(J - K) = 2.93$ for $[\text{Fe}/\text{H}] = -0.5$, $(m - M)_0 = 13.70$ and $E(J - K) = 2.81$ for $[\text{Fe}/\text{H}] = -1.0$, or $(m - M)_0 = 14.43$ and $E(J - K) = 2.70$ for $[\text{Fe}/\text{H}] = -2.0$, while Borissova et al. (2007) found $(m - M)_0 = 13.60$ and $E(J - K) = 2.98$ for a disk-like enrichment scenario, or $(m - M)_0 = 13.48$ and $E(J - K) = 3.01$ for a bulge-like one.

To start our analysis of 2MASS-GC02, we built the cluster CMDs for the various available filter combinations from our VVV photometry. In Figure 1, we show the K_s vs. $J - K_s$ CMD. Stars inside the half-light radius, plotted with bigger solid squares, allow us to distinguish the red-giant branch (RGB) of the cluster, with a clump at $K_s \approx 14$ and $J - K_s \approx 3.2$, but do not reach the main-sequence (MS) turn-off point. In addition, 2MASS-GC02 is poorly-populated, and it lies in a region of high field stellar densities, so including in the CMD stars located farther away from the cluster center, but still well within its tidal radius – which in other cases, like halo GCs surrounded by fields with small stellar densities, would help to increase the definition of the RGB branch –, here only makes the task of analyzing the cluster CMD more difficult. The elevated number of bulge field giants present, lying in the same CMD region where the cluster stars are located, adds confusion to the study of 2MASS-GC02. The presence of significant differential extinction in the field, clearly shown by the broadenings in the RGB and red clump (RC) of the bulge

stars present, complicates even more the CMD analysis. To complete the description of the observed CMD, we should mention that a significant number of field, main-sequence disk stars can be observed as a clear branch of stars bluer than $J - K_s < 2$. A deeper, more quantitative analysis of the cluster CMD will probably not allow us to extract the physical parameters of the cluster with better accuracy than previous photometric studies down to similar magnitude depths (Ivanov et al. 2000; Borissova et al. 2007). Instead, we decided to take advantage of our multi-epoch variability survey and use it to extract these physical parameters from the information provided by the RR Lyrae contained in the cluster.

4.1. Variables in 2MASS-GC02

There are observations in K_s in 43 different epochs for 2MASS-GC02 during the period 2010-2013 of the VVV survey (see Table 2), although we only considered 42 in our following analysis since tracking problems during the observations of one set produced very elongated stars that were unusable for our variability study. We more than triple the number of epochs in the only previous variability study of this cluster, performed by Borissova et al. (2007), with only 13 epochs. They found 5 RR Lyrae variable candidates, but our improved photometry and temporal coverage shows that none of them is a true variable star⁶. Fortunately, after performing the variability analysis described in Section 3, we were able to find 32 new variable candidates inside the tidal radius. Among them, we identified 13 RR Lyrae variables, 3 Cepheids, 4 eclipsing binaries, and 3 LPVs. Their positions, periods, amplitudes, magnitudes and colors are shown in Table 3 (NV1 to NV32), their light curves are plotted in Figure 2, their positions on the sky can be observed in Figure 3, and their positions in the CMD can be observed in the left panel of Figure 1.

All of the RR Lyrae candidates found (NV1 to NV10, NV13, NV24 and NV26) seem to be RRab's according to their periods and light curves. From their position in the CMD and on the sky, it is immediately clear that the RR Lyrae candidates towards the north of the cluster center (NV4, NV7, NV9 and NV13) have redder colors, and therefore seem to be more severely affected by extinction, than the RRab candidates in the south (NV1, NV2, NV5, NV6, NV8). This feature points towards significant differential extinction across the face of the cluster. From their position in the different available CMDs, all the RRab candidates seem to belong to the cluster except NV26 – we will further confirm this point in Section 4.3. NV26 is approximately half a magnitude dimmer than the other RRab variables with similar colors, which implies that the increase in magnitude is not due to higher reddening. This feature, clearly observable in Figure 4, along with being the one farthest away from the cluster center and having a period significantly shorter than most of the other RRab candidates, suggest it is a background field RR Lyrae.

The Cepheid candidates NV11, NV28, and NV31 show periods between ≈ 1 and ≈ 10 days, and light curves

⁶ Although our NV2 and their V3 RR Lyrae could be in principle cross-matched, they are already $3.1''$ away, i.e., separated by more than 9 pixels in the VVV images, and the reported periods and average magnitudes are quite different.

with a sawtooth shape, characteristic of these stars in K_s (Angeloni et al. 2014). Unfortunately, none of them seem to have high chances to belong to the cluster. NV11 and NV28 are too dim to be Type II Cepheids belonging to 2MASS-GC02. According to the period-luminosity relations by Matsunaga et al. (2013), their apparent distance moduli are $\mu_{\text{NV11}} = 17.80$ and $\mu_{\text{NV28}} = 16.76$, which differ significantly from those of the RR Lyrae shown in Figure 4 – the method to obtain those is explained in Section 4.3. Their position in the CMD suggest they are background bulge field Cepheids. On the other hand, NV31 has $\mu_{\text{NV31}} = 15.57$, according to the period-luminosity relations by Matsunaga et al. (2013) for Type II Cepheids. This apparent distance modulus is in the range shown by the RR Lyrae in the GC (see Figure 4), but as shown in the CMD in Figure 1, its color is too blue for NV31 to belong to the cluster or bulge.

The eclipsing binary candidates NV12, NV20, NV22, and NV32 have light curve characteristics of Algol-type binaries (EA). NV32 is too blue to be a cluster member based on its position in the CMD, but the remaining EA candidates cannot be disregarded as cluster members from the CMD examination since they lie in regions where there are cluster stars.

At the present time, there is not much we can say about the 3 LPVs discovered, NV16, NV19 and NV27. Their long periods have not allowed us yet to sample their light curves with enough phase coverage for an accurate period determination. Also their red colors seem to be the reason NV16 has been detected only in K_s , NV27 in H and K_s , and NV19 in J , H and K_s .

Almost all of the remaining 9 unclassified variables seem to be disk field stars based on their position in the CMD. The only one that could be a cluster member is NV29.

4.2. Variables surrounding 2MASS-GC02

As previously mentioned in Section 2, we performed a search for variables out to a radius of $10'$ from the cluster center. This allowed us to look for variables in the field surrounding the GC, in an area approximately 3 times the size of the cluster. We found a total of 70 new variable candidates in this surrounding region. Their positions, periods, amplitudes, magnitudes and colors are shown in Table 3 (NV33 to NV102), their light curves are plotted in Figure 2, their positions on the sky can be observed in Figure 3, and their positions in the CMD can be observed in the right panel of Figure 1.

We found 6 extra-tidal RR Lyrae (NV70, NV72, NV76, NV77, NV85, and NV99) in the region studied outside the tidal radius. From the shape of their light curve and their periods they are RRab's. From their position in the CMD all of them are clearly in the background of the GC, except NV85 and NV99 – we will further confirm this point in Section 4.3–. The high angular separations from the center of the cluster (see Table 3) and the positions in the sky (see Figure 3) of NV85 and NV99 suggest that, instead of being variables in a hypothetical GC tidal tail, they have a higher chance of being field stars located at a distance similar to that of the cluster. Most of the found field RR Lyrae being in the background of the cluster, points towards 2MASS-GC02 being in front –or in the near-side– of the Galactic bulge.

In addition to these 6 RR Lyrae, we also identified 6

Cepheids, 4 eclipsing binaries, and 19 LPV candidates. From a purely statistical point of view, being the surrounding area 3 times bigger than the region inside the tidal radius, we should expect 2 field RR Lyrae, 2 field Cepheids, 1 field eclipsing binaries, and 6 field LPV candidates inside the cluster radius. These numbers of variables are within the range of these objects found in Section 4.1, given that we are dealing with small number statistics, except for the case of RR Lyrae, where we find many more (however, it agrees with the number of field RR Lyrae found in Section 4.1). Therefore, this strengthens our assumption that most of the inner RR Lyrae candidates found in Section 4.1 are cluster members, and most, if not all, of the inner Cepheids, eclipsing binaries, and LPV candidates are field stars.

4.3. Distance, reddening and Oosterhoff type

The reddening values and distances of every individual RRab star can be accurately calculated using their tight period-luminosity-metallicity relations in the near-infrared (Longmore et al. 1986, 1990; Bono et al. 2001; Cassisi et al. 2004; Catelan et al. 2004). Following the steps detailed in Dékány et al. (2013), we adapted the Catelan et al. (2004) period-luminosity relations to be used with the VIRCAM/VISTA filter system:

$$M_{K_s} = -0.6365 - 2.347 \log(P) + 0.1747 \log(Z) \quad (1)$$

$$M_H = -0.5539 - 2.302 \log(P) + 0.1781 \log(Z) \quad (2)$$

$$M_J = -0.2361 - 1.830 \log(P) + 0.1886 \log(Z) \quad (3)$$

$$M_Y = +0.0090 - 1.467 \log(P) + 0.1966 \log(Z) \quad (4)$$

$$M_Z = +0.1570 - 1.247 \log(P) + 0.2014 \log(Z) \quad (5)$$

where P is the period of the RRab and Z its metallicity.

The only spectroscopic determination of the iron content for the stars in 2MASS-GC02 we have found in the literature is by Borissova et al. (2007). They found a value of $[\text{Fe}/\text{H}] = -1.08$, using low-resolution infrared spectroscopy of secondary lines in a set of 12 cluster stars, selected by their photometry and radial velocities⁷. Although photometric estimations are a little higher, with values between $[\text{Fe}/\text{H}] = -0.66$ (Borissova et al. 2002) to $[\text{Fe}/\text{H}] = -0.98$ (Borissova et al. 2007), we decided to stick to the spectroscopic value, which is also the one provided by the Harris (1996) catalog (see Table 1). Using a canonical helium fraction $Y = 0.245$, and an alpha-element enhancement $[\alpha/\text{Fe}] = 0.3$, common among Galactic GCs (Pritzl et al. 2005), we translate the iron content $[\text{Fe}/\text{H}] = -1.08$ to the metallicity $Z = 0.0025$ that we will assume for all the RRab stars in the cluster.

It is straightforward to calculate the apparent distance modulus of the RRab candidates in K_s (see Figure 4), using the calculated period and average apparent magnitudes in Table 3. But to calculate the absolute distance modulus we need to carry out some further calculations and adopt some further assumptions in order to obtain the extinction first. Ideally to calculate the extinction, we should also have the light curve in some other near-infrared filter in addition to K_s , but VVV only provides single-epoch observations in Z , Y , J , and H . What is

worse, the Z and Y magnitudes of the RR Lyrae candidates in 2MASS-GC02 are in most cases below the detection limit (see Table 3). For our analysis, we assume that $J - K_s$ (or $H - K_s$) at the phase position when the J (or H) image was taken is equal to the average $J - K_s$ (or $H - K_s$) color of the RR Lyrae candidate. We obtain the K_s value at the desired phase from our Fourier fits to the light curves for the RRab candidates (see Section 3), calculate this way the apparent colors of these RR Lyrae candidates, shown in Table 3, and using equations 3 to 5 obtain their color excesses $E(J - K_s)$ and $E(H - K_s)$, shown in Figure 4.

Now, in order to obtain the absolute distance modulus to 2MASS-GC02 we should transform those color excesses to extinctions using the total-to-selective extinction ratios. But these ratios have been shown to differ from the values obtained from the standard Cardelli et al. (1989) extinction law, when observing towards the Galactic center and bulge (e.g. Nishiyama et al. 2006, 2009). Therefore, instead of adopting a ratio from the literature, the highly differential reddening inside the cluster's area enables us to simultaneously obtain the absolute distance modulus and the total-to-selective extinction ratio (and hence the extinction) by doing a linear fit between the two parameters we already had, the apparent distance modulus $K_s - M_{K_s}$ and the color excess ($E(J - K_s)$ and $E(H - K_s)$). Since there are errors associated with both variables, the fit is performed using the ordinary least square bisector method, which has been proven to outperform other approaches in such cases (Isobe et al. 1990; Kunder et al. 2008). The fits are shown in Figure 4. As we can expect, most RR Lyrae outside the tidal radius are obvious outliers in the fit, and can be clearly located in the background of the cluster (see Section 4.2). From the RR Lyrae inside the tidal radius, only NV26 has been also considered to be an outlier, due to its considerable residuals, and was discarded from the fitted sample (see discussion and explanations for these cases in Section 4.1). From the final fit, we obtain the ratios $R_{K_s, J-K_s} \equiv \mathcal{A}_{K_s} / (E(J - K_s))$ and $R_{K_s, H-K_s} \equiv \mathcal{A}_{K_s} / (E(H - K_s))$ shown in Table 4. These ratios are a little lower than those obtained by Nishiyama et al. (2009), and are certainly smaller than suggested by Cardelli et al. (1989) or Rieke & Lebofsky (1985). The absolute distance modulus, calculated as the average of the zero-points of the fits, is $\mu_0 = 14.26 \pm 0.14 \pm 0.3$, where the first σ is obtained from the statistical errors in the fit, and the second one comes from omitting some of the fitted stars, as we explained in the following paragraph. This value for the absolute distance modulus yields the cluster's distances to the Sun and to the Galactic center shown in Table 5, putting the object farther away from us and more than 1 kpc closer to the Galactic center than shown in the Harris (1996) catalog. For the sake of comparison, we chose as a good reference value for the extinction towards 2MASS-GC02 $E(J - K_s) = 3.1 \pm 0.5$, the mean of the cluster RRab candidates, but we would like to remark that extinction towards this cluster is highly variable, with almost 50% changes over small regions, and with significant deviations from the standard extinction law.

The assumption of $\mathcal{A}_\lambda / \mathcal{A}_{K_s} = 1$ that we have done by using only one epoch in J and H in order to obtain the colors of the RR Lyrae, does not add significantly

⁷ Peñaloza et al. (in preparation) also report a value of $[\text{Fe}/\text{H}] = -1.08$ from high-resolution spectra of a few cluster giants.

to the error budget of the different calculated magnitudes. Using the relations from Appendix B1.3 in Feast et al. (2008), we observed that the ratios between the amplitudes of the RR Lyrae in the near-infrared change according to the amplitudes of the RR Lyrae, and for the amplitudes of the detected RR Lyrae (see Table 3), the values⁸ should be in the ranges $0.9 < \mathcal{A}_H/\mathcal{A}_K < 1.1$ and $0.8 < \mathcal{A}_J/\mathcal{A}_K < 1.9$, and the errors in the RR Lyrae colors due to our assumption could be, at most, of one tenth of a magnitude in $J - K_s$, and one hundredth of a magnitude in $H - K_s$. Note however that these would be the extreme cases when the measurements were taken at a phase corresponding to a maximum or a minimum; generally the error should be smaller, and their effect on the elevated color excesses that we obtained (see Figure 4) almost negligible. What is more, any effects from our assumption of $\mathcal{A}_\lambda/\mathcal{A}_{K_s} = 1$ would cancel out to some extent in the fit we have done to obtain the absolute distance modulus and the reddening law, since the measurements of J and H were done at random phase times, which means that errors in color excesses should have similar chances of being positive and negative, and the only observable effect would be a small increase in the dispersion of the points around the fit. More important for the error budget of the extinction ratios R and the absolute distance modulus μ_0 would be if one of the fitted RR Lyrae with a higher extinction (NV4 or NV7) resulted not to be a member of the cluster. Since they present the highest deviations from the fit, and they are also important to extend the extinction baseline, we decided to show the effects of omitting one of them as the variations shown by the second term in the error of the extinction ratios R and the absolute distance modulus μ_0 .

The average period of the cluster RRab candidates used in the fit (NV1-NV10, NV13 and NV24) is $\langle P_{ab} \rangle = 0.59 \pm 0.06$ days, which puts 2MASS-GC02 in the Oosterhoff gap, as we can see in Figure 5. Based on the absence of Galactic GCs in this gap, and their high incidence in nearby extragalactic systems (see Figure 5), this feature could suggest an extragalactic origin for 2MASS-GC02. However, we should note that we are dealing with small number statistics here, since only 12 RRab's are considered.

5. TERZAN 10

Since its discovery by Terzan (1971), there have been only a few photometric studies published on Terzan 10 – e.g., Liu et al. (1994) in the near-infrared, Ortolani et al. (1997) in the optical; and no spectroscopic studies of its individual stars, although Bica et al. (1998) studied the integrated spectra of this GC. Estimations of the reddening range from $E(B - V) = 1.71$ (Webbink 1985) or $E(B - V) = 1.90$ (Bica et al. 1998) to $E(B - V) = 2.40$ (Ortolani et al. 1997) or $E(B - V) = 2.60$ (Liu et al. 1994). Its distance modulus estimations also show a significant range, varying from $(m - M)_0 = 13.40$ (Ortolani et al. 1997) to $(m - M)_0 = 14.5$ (Liu et al. 1994).

In Figure 6, we show the K_s vs. $J - K_s$ CMD of the cluster that we built with our VVV PSF photome-

try. It is immediately clear that, although extinction is lower than for 2MASS-GC02 (see Figure 1), it is difficult to disentangle cluster stars from their field counterparts. Even at distances smaller than the half-light radius, plotted with bigger solid squares in the left panel of Figure 6, there is a significant presence of disk and bulge field populations in addition to the GC. The RGB of the cluster, with a clump at $K_s \approx 13.5$ and $J - K_s \approx 1.5$, is mixed with bulge field giants. The brightest disk field stars are bluer than the upper RGB stars ($J - K_s < 1.2$) and can be easily separated from them, but the dimmest disk field stars contribute to the confusion caused by the bulge field stars, since both are located in the same region as the subgiant branch (SGB) and upper MS of the cluster. Therefore, even though our photometry reaches the turn-off point of the MS, we cannot properly define it due to the contamination by the field populations. Again, instead of trying to perform a deeper CMD analysis and statistical field star decontamination, we decided to take advantage of our variability survey and use it to extract Terzan 10 physical parameters from the information provided by the RR Lyrae variables we identified in the cluster.

5.1. Variables in Terzan 10

Observations in K_s were taken in 101 different epochs for Terzan 10 during the period 2010-2013 of the VVV survey (see Table 2), making this region one of the most sampled in the VVV so far. No previous search for variable stars in this cluster has been ever done⁹, so this high amount of available epochs puts us in a superb position to find for the first time highly significant variable candidates in this GC. Our analysis resulted in 48 variable candidates inside $r_t = 5.06'$, the tidal radius extracted from the Harris (1996) catalog. Among the 48 candidates, we identified 8 RR Lyrae variables, 8 Cepheids, 7 eclipsing binaries, and 1 LPV. Their positions, periods, amplitudes, magnitudes and colors are shown in Table 6 (NV1 to NV48), their light curves are plotted in Figure 7, their positions in the sky can be observed in Figure 8, and their positions in the CMD can be observed in the left panel of Figure 6.

All of the RR Lyrae candidates found (NV2, NV3, NV5, NV6, NV7, NV12, NV22 and NV24) seem to be RRab's, according to their periods and light curves.

⁹ During the revision process of our article, Soszyński et al. (2014) published their results on the RR Lyrae in the OGLE Galactic Bulge fields. Since Terzan 10 falls on one of the fields covered by OGLE-IV, we matched their results with ours, and found that most of the RRab's in the field of Terzan 10 and in its surroundings appear in both works. There are only 3 RRab candidates inside the cluster radius of Terzan10 (OGLE_BLG_RRLYR-33521, OGLE_BLG_RRLYR-33518, and OGLE_BLG_RRLYR-33525), and 1 RRab candidate in the surrounding region (OGLE_BLG_RRLYR-33508) that Soszyński et al. (2014) find, and we do not. The reason for this is that these stars lie very close to stars of similar or higher magnitude, and the image subtraction technique they use is better suited than our PSF photometry technique in this case. On the other hand, there are 1 RRab candidate inside the tidal radius of Terzan 10 (NV5) and 1 in the surrounding region (NV140) that we identify and they do not. The reason for this is their dimmer magnitudes in I , close to the magnitude limit where the completeness of the OGLE detection is small. We should also note that we are not able to recover any of the 7 RRc candidates that Soszyński et al. (2014) find in Terzan 10 and its surroundings, due to the smaller amplitudes of these variable stars in the near-infrared wavelengths.

⁸ A similar value for $\mathcal{A}_J/\mathcal{A}_{K_s}$ is obtained by Navarrete et al. (in preparation) when studying the RR Lyrae light curves in the near-infrared in OmegaCen.

From their position in the CMD and in the sky, the RR Lyrae are located along the reddening vector, suggesting the presence of differential extinction in this GC, with the candidates towards the north of the cluster center (NV3 and NV5) with redder colors, and therefore more heavily affected by extinction, than the RRab candidates in the south (NV2, NV6, NV7 and NV12). On the CMD, we can observe that all RR Lyrae show a behavior consistent with their belonging to the cluster and following the same, but again non-standard, reddening law, except NV12 – we will further confirm this point in Section 5.3. NV12 is a little brighter than the other RR Lyrae with similar colors, which suggests that it is a foreground RR Lyrae star.

None of the Cepheid candidates found (NV14, NV16, NV17, NV18, NV19, NV31, NV39 and NV47) could be a Cepheid that belongs to the cluster according to the Matsunaga et al. (2013) period-luminosity relations. While most of them are too dim to even belong to the Galactic bulge, NV16 and NV17 have apparent distance moduli consistent with being bulge Type II Cepheids ($\mu_{\text{NV16}} = 15.98$ and $\mu_{\text{NV17}} = 14.98$), along with positions in the CMD accordant with it. But they do not seem to belong to Terzan 10 either. A quick visual comparison with the RR Lyrae apparent distance moduli and extinctions shown in Figure 9 – the method to obtain them is explained in Section 5.3 – strongly points towards NV16 being a Type II Cepheid in the background of the cluster, and NV17 being in its foreground.

All the eclipsing binary candidates (NV1, NV4, NV20, NV23, NV32, NV41, and NV45) lie in a region of the CMD compatible with being cluster members, except NV4 and NV23, which are located among the disk field stars. Based on their light curves most of them appear to be EA stars.

Only 1 LPV was found inside the tidal radius of the cluster, NV48. Its long period precludes us from having a well-sampled light curve.

The vast majority of the remaining 23 unclassified variables, seems to be comprised of disk field variables, based on their positions in the CMD (see Figure 6).

5.2. Variables surrounding Terzan10

For Terzan 10, we also performed a search for variables in the immediate surrounding of the cluster, out to a radius of $10'$ from its center. This encircles an area approximately 3 times the size of the cluster out to its tidal radius. In this region we found 112 more variable candidates. Their positions, periods, amplitudes, magnitudes and colors are shown in Table 6 (NV49 to NV160), their light curves are plotted in Figure 7, and their positions in the CMD can be observed in the right panel of Figure 6.

We found 12 RR Lyrae candidates in the surveyed region, significantly more than the RR Lyrae found in the surrounding of 2MASS-GC02. But extinction in that region was higher, as we can guess just by looking at the redder colors of the stars there, and the angular separation from the Galactic center was also higher, meaning that less of the projected bulge was sampled. In general, RR Lyrae found in the surroundings of Terzan 10 are a little brighter than the ones found inside its tidal radius, and their colors are similar, which suggests similar reddenings. These two facts imply that they are field

RR Lyrae in the foreground of the cluster, suggesting that the cluster is on the far side of the bulge, farther away than the Galactic center. We will confirm this result and further discuss it in Section 5.3. From the CMD and from the further analysis in Section 5.3, only one of the RR Lyrae, NV140, is behind the cluster, and other two, NV105 and NV136, lie at a distance consistent with being cluster members, although their high angular distances from the cluster center make more probable that they are field stars at the cluster’s distance. From a statistical point of view, the expected number of field RR Lyrae inside the cluster radius should be ≈ 4 , since the surrounding region is 3 times the area occupied by the cluster. Although we only found 1 (see Section 5.1), we should note that we are dealing with small number statistics here.

We also identified 15 Cepheids, 27 eclipsing binaries, and 2 LPVs. Therefore, we should expect in the area inside the cluster tidal radius close to 5 field Cepheids, 9 field eclipsing binaries and 1 field LPV, given the bigger size of the surrounding region (3:1). The amounts of these kinds of variables found in Section 5.1 (8 Cepheids, 7 eclipsing binaries and 1 LPV) are of the same order, suggesting that most, if not all, of the variables of these types found in Section 5.1 belong to the field population, and not to the cluster.

The number of LPVs seems odd when compared with 2MASS-GC02. There we found 19 LPVs, while in the surrounding of Terzan 10 we found only 2.

5.3. Distance, reddening and Oosterhoff type

To calculate the distance and the extinction to Terzan 10 we follow the same steps as in Section 4.3. We use equations 1 to 5 to obtain the absolute magnitudes of our RR Lyrae candidates in the different available filters. Unfortunately, we found no spectroscopic metallicity measurements of individual stars in Terzan 10, and we have to rely on only photometric and integrated spectroscopic values. Metallicity estimations vary between $[\text{Fe}/\text{H}] = -0.7$ in the photometric studies by Liu et al. (1994) to $[\text{Fe}/\text{H}] = -1.2$ ($[Z/Z_{\odot}] = -1.35$) in the integrated spectroscopic studied by Bica et al. (1998). We adopt $[\text{Fe}/\text{H}] = -1.00$, from the Harris (1996) catalog, and assuming the same Y and α -enhancement as in Section 4.3, we obtain a value of $Z = 0.003$ for the cluster’s metallicity, that we used as input for equations 1 to 5, along with our measured periods. The mean RR Lyrae apparent K_s magnitude is obtained as mentioned in Section 3, and the apparent colors from the K_s measurements obtained by interpolating in our Fourier fit to the K_s light curve at the same phase as the single-epoch images in Z , Y , J , and H were taken.

As in Section 4.3, we did not assume an a priori extinction law to relate color excess with apparent distance modulus of the RRab candidates. Instead, using the ordinary least square bisector method, we got a linear fit between both parameters, which provide us with values for the extinction ratios $R_{K_s, \lambda - K_s}$, as the slope of the fit, and an absolute distance modulus, as the zero-point of the fit (see Figure 9). In our analysis, the only clear outlier among the RR Lyrae inside the tidal radii, and therefore excluded from the fit, was NV12 (see discussion in Section 5.1). Some of the RR Lyrae in the surrounding field outside the tidal radius could belong to the cluster

according to their distances, although this is not very plausible (see discussion in Section 5.2). Again, the ratios $R_{K_s, \lambda-K_s}$ derived from the fit differ from those of the standard Cardelli et al. (1989) law, and agree better with those derived by Nishiyama et al. (2009), as we can see in Table 4. The fact that the zero-point of the fits, i.e., the absolute distance modulus, show a much smaller spread among the values derived from using the different filter-combinations, than if we just use the Cardelli et al. (1989) law (see Figure 9), reinforces our confidence in the fitted values. We adopt the weighted average of the zero-points from the different color-excess fits, as the absolute distance modulus of Terzan 10. We obtain a value $\mu_0 = 15.06 \pm 0.03 \pm 0.03$, where again the first σ is obtained from the statistical errors in the fit, while the second one comes from omitting two of the fitted stars, NV22 and NV5, which have the smallest and biggest extinction values. This value of μ_0 implies the cluster is much farther away from us than previously thought, almost by a factor of 2 (see Table 5). This also implies that Terzan 10 is beyond the Galactic center, in the far side of the Galactic bulge. Until now it was believed that all the inner Galactic GCs found so far were located in the near side of the bulge (Barbuy et al. 1998). For the sake of comparison, a good reference value for the extinction towards Terzan 10 is $E(J - K_s) = 0.86 \pm 0.16$, the mean of the cluster RRab candidates that made our fit, but we emphasize that extinction towards this cluster is also highly variable, with almost 50% changes over small regions, and with significant deviations from the standard extinction law.

The average period of Terzan 10 RRab variable candidates used in the fit (NV2, NV3, NV5, NV6, NV7, NV22 and NV24) is $\langle P_{ab} \rangle = 0.66 \pm 0.06$ days, which makes Terzan 10 an Oosterhoff II cluster. However, its iron-content is significantly higher than the ones of the other Galactic (and even extragalactic) Oosterhoff II GCs (see Figure 5). But we should remember here that the metallicity value adopted in this work is the average of two previous works ($[\text{Fe}/\text{H}] = -0.7$ by Liu et al. (1994), and $[\text{Fe}/\text{H}] = -1.2$ by Bica et al. (1998)), as we mentioned in the beginning of this section. If $[\text{Fe}/\text{H}] = -0.7$ is closer to the true value, this will put Terzan 10 closer to NGC 6388 and NGC 6441, in the scarcely populated Oosterhoff III group of metal-rich clusters with RR Lyrae. If, on the other hand, $[\text{Fe}/\text{H}] = -1.2$ is closer to reality, Terzan 10 would still be the most metal-rich cluster in the Oosterhoff II group, and would still stand out significantly from the locus of Galactic GCs. This uncertainty makes a strong case to obtain spectroscopic metallicity measurements from individual stars in this GC.

6. SUMMARY

We have shown the potential of the VVV survey for studying the variable stars of the inner Galactic GCs, by analyzing two highly-reddened GCs of this sample, 2MASS-GC02 and Terzan 10. We have discovered 32 new variables inside the tidal radius of 2MASS-GC02 and 70 in a close surrounding region, while for Terzan 10 we have found 48 new variables inside its tidal radius, and 112 in its immediate surroundings. In both GCs, we have found a significant number of fundamental-mode RR Lyrae (12 in 2MASS-GC02, 7 in Terzan 10) that we have used to accurately measure the extinctions and distances of these GCs, and to explore the non-standard extinction law in their directions. Both clusters are closer to the Galactic center than previously thought ($R_{GC} = 1.8$ kpc for 2MASS-GC02; $R_{GC} = 2.1$ kpc for Terzan 10). We have also found Terzan 10 to be beyond the Galactic center, making it the only currently known GC to be on the far side of the Galactic bulge. Extinction towards both clusters is elevated (especially towards 2MASS-GC02) and highly differential, and it follows a non-standard law, with values for the selective-to-total extinction ratios similar to those quoted by Nishiyama et al. (2009). We have also found both clusters to have quite uncommon Oosterhoff properties. Terzan 10 can be one of the most metal-rich Oosterhoff II GCs found in the Galaxy, or belong to the scarcely-populated metal-rich Oosterhoff III group, depending on the true metallicity of this cluster. The latter case would imply a possible He self-enrichment scenario, in analogy to the other two Oosterhoff III GCs (see Catelan (2009a), for a review and extensive references). 2MASS-GC02, on the other hand, is located in the Oosterhoff gap where very few of the Galactic globular clusters lie, which may suggest an extragalactic origin for this GC.

There are 34 more known inner Galactic GCs covered by the VVV survey, and the study of their variable stars, which we plan to present in future papers in this series, will greatly contribute to better establish their physical parameters, and to understand the origin of the Oosterhoff dichotomy in our Galaxy.

We thank Andrzej Udalski for his help comparing some of our detected variables with unpublished OGLE data to better determine their variability type. This project is supported by the Chilean Ministry for the Economy, Development, and Tourism's Programa Iniciativa Científica Milenio through grant IC120009, awarded to the Millennium Institute of Astrophysics (MAS); by Proyecto Fondecyt Postdoctoral 3130552 and 3140575; by Proyecto Fondecyt Regular 1141141; by CONICYT-PCHA Magíster Nacional 2014-22141509; and by the ALMA-CONICYT project 31110002.

Facility: ESO:VISTA (VIRCAM).

REFERENCES

- Alonso-García, J., Mateo, M., Sen, B., et al. 2012, *AJ*, 143, 70
 Angeloni, R., Contreras Ramos, R., Catelan, M., et al. 2014, *A&A*, 567, A100
 Barbuy, B., Bica, E., & Ortolani, S. 1998, *A&A*, 333, 117
 Bica, E., Claria, J. J., Piatti, A. E., & Bonatto, C. 1998, *A&AS*, 131, 483
 Bono, G., Caputo, F., Castellani, V., Marconi, M., & Storm, J. 2001, *MNRAS*, 326, 1183
 Borissova, J., Ivanov, V. D., Stephens, A. W., et al. 2007, *A&A*, 474, 121
 Borissova, J., Ivanov, V. D., & Vanzani, L. 2002, in *IAU Symposium*, Vol. 207, *Extragalactic Star Clusters*, ed. D. P. Geisler, E. K. Grebel, & D. Minniti, 107
 Caloi, V., & D'Antona, F. 2007, *A&A*, 463, 949
 Cardelli, J. A., Clayton, G. C., & Mathis, J. S. 1989, *ApJ*, 345, 245

- Cassisi, S., Castellani, M., Caputo, F., & Castellani, V. 2004, *A&A*, 426, 641
- Catelan, M. 2009a, *Ap&SS*, 320, 261
- Catelan, M. 2009b, in *IAU Symposium*, Vol. 258, IAU Symposium, ed. E. E. Mamajek, D. R. Soderblom, & R. F. G. Wyse, 209–220
- Catelan, M., Pritzl, B. J., & Smith, H. A. 2004, *ApJS*, 154, 633
- Catelan, M., Minniti, D., Lucas, P. W., et al. 2011, in *RR Lyrae Stars, Metal-Poor Stars, and the Galaxy*, ed. A. McWilliam, 145
- Catelan, M., Minniti, D., Lucas, P. W., et al. 2013, *ArXiv e-prints*, arXiv:1310.1996
- Clement, C. M., Muzzin, A., Dufton, Q., et al. 2001, *AJ*, 122, 2587
- Corwin, T. M., Sumerel, A. N., Pritzl, B. J., et al. 2006, *AJ*, 132, 1014
- Dékány, I., Minniti, D., Catelan, M., et al. 2013, *ApJ*, 776, L19
- Emerson, J. P., Irwin, M. J., Lewis, J., et al. 2004, in *Society of Photo-Optical Instrumentation Engineers (SPIE) Conference Series*, Vol. 5493, *Optimizing Scientific Return for Astronomy through Information Technologies*, ed. P. J. Quinn & A. Bridger, 401–410
- Feast, M. W., Laney, C. D., Kinman, T. D., van Leeuwen, F., & Whitelock, P. A. 2008, *MNRAS*, 386, 2115
- Gillessen, S., Eisenhauer, F., Trippe, S., et al. 2009, *ApJ*, 692, 1075
- Hambly, N. C., Mann, R. G., Bond, I., et al. 2004, in *Society of Photo-Optical Instrumentation Engineers (SPIE) Conference Series*, Vol. 5493, *Optimizing Scientific Return for Astronomy through Information Technologies*, ed. P. J. Quinn & A. Bridger, 423–431
- Harris, W. E. 1996, *AJ*, 112, 1487
- Hurt, R. L., Jarrett, T. H., Kirkpatrick, J. D., et al. 2000, *AJ*, 120, 1876
- Irwin, M. J., Lewis, J., Hodgkin, S., et al. 2004, in *Society of Photo-Optical Instrumentation Engineers (SPIE) Conference Series*, Vol. 5493, *Optimizing Scientific Return for Astronomy through Information Technologies*, ed. P. J. Quinn & A. Bridger, 411–422
- Isobe, T., Feigelson, E. D., Akritas, M. G., & Babu, G. J. 1990, *ApJ*, 364, 104
- Ivanov, V. D., Borissova, J., & Vanzì, L. 2000, *A&A*, 362, L1
- Kovács, G., Bakos, G., & Noyes, R. W. 2005, *MNRAS*, 356, 557
- Kunder, A., Popowski, P., Cook, K. H., & Chaboyer, B. 2008, *AJ*, 135, 631
- Liu, T., McLean, I., & Becklin, E. 1994, in *Astrophysics and Space Science Library*, Vol. 190, *Astronomy with Arrays, The Next Generation*, ed. I. S. McLean, 101
- Longmore, A. J., Dixon, R., Skillen, I., Jameson, R. F., & Fernley, J. A. 1990, *MNRAS*, 247, 684
- Longmore, A. J., Fernley, J. A., & Jameson, R. F. 1986, *MNRAS*, 220, 279
- Matsunaga, N., Feast, M. W., Kawadu, T., et al. 2013, *MNRAS*, 429, 385
- Minniti, D., Lucas, P. W., Emerson, J. P., et al. 2010, *New Astronomy*, 15, 433
- Minniti, D., Hempel, M., Toledo, I., et al. 2011, *A&A*, 527, A81
- Moni Bidin, C., Mauro, F., Geisler, D., et al. 2011, *A&A*, 535, A33
- Nishiyama, S., Tamura, M., Hatano, H., et al. 2009, *ApJ*, 696, 1407
- Nishiyama, S., Nagata, T., Kusakabe, N., et al. 2006, *ApJ*, 638, 839
- Oosterhoff, P. T. 1939, *The Observatory*, 62, 104
- Ortolani, S., Bica, E., & Barbuy, B. 1997, *A&AS*, 126, 319
- Pritzl, B., Smith, H. A., Catelan, M., & Sweigart, A. V. 2000, *ApJ*, 530, L41
- Pritzl, B. J., Smith, H. A., Catelan, M., & Sweigart, A. V. 2001, *AJ*, 122, 2600
- . 2002, *AJ*, 124, 949
- Pritzl, B. J., Smith, H. A., Stetson, P. B., et al. 2003, *AJ*, 126, 1381
- Pritzl, B. J., Venn, K. A., & Irwin, M. 2005, *AJ*, 130, 2140
- Rieke, G. H., & Lebofsky, M. J. 1985, *ApJ*, 288, 618
- Saito, R. K., Minniti, D., Dékány, I., et al. 2011, in *Revista Mexicana de Astronomía y Astrofísica Conference Series*, Vol. 40, *Revista Mexicana de Astronomía y Astrofísica Conference Series*, 221–224
- Saito, R. K., Hempel, M., Minniti, D., et al. 2012, *A&A*, 537, A107
- Schechter, P. L., Mateo, M., & Saha, A. 1993, *PASP*, 105, 1342
- Smith, H. A., Catelan, M., & Kuehn, C. 2011, in *RR Lyrae Stars, Metal-Poor Stars, and the Galaxy*, ed. A. McWilliam, 17
- Soszyński, I., Udalski, A., Szymański, M. K., et al. 2014, *Acta Astron.*, 64, 177
- Stellingwerf, R. F. 1978, *ApJ*, 224, 953
- Stetson, P. B. 1996, *PASP*, 108, 851
- Taylor, M. B. 2006, in *Astronomical Society of the Pacific Conference Series*, Vol. 351, *Astronomical Data Analysis Software and Systems XV*, ed. C. Gabriel, C. Arviset, D. Ponz, & S. Enrique, 666
- Terzan, A. 1971, *A&A*, 12, 477
- Valenti, E., Ferraro, F. R., & Origlia, L. 2007, *AJ*, 133, 1287
- Webbink, R. F. 1985, in *IAU Symposium*, Vol. 113, *Dynamics of Star Clusters*, ed. J. Goodman & P. Hut, 541–577
- Welch, D. L., & Stetson, P. B. 1993, *AJ*, 105, 1813
- Yoon, S.-J., Joo, S.-J., Ree, C. H., et al. 2008, *ApJ*, 677, 1080
- Yoon, S.-J., & Lee, Y.-W. 2002, *Science*, 297, 578
- Zechmeister, M., & Kürster, M. 2009, *A&A*, 496, 577

TABLE 1
PHYSICAL PARAMETERS OF THE STUDIED CLUSTERS, ACCORDING TO THE 2010 VERSION OF THE HARRIS (1996) CATALOG.

Cluster	l (deg)	b (deg)	[Fe/H]	M_V	r_h (arcmin)	r_t (arcmin)
2MASS-GC02	9.79	-0.61	-1.08	-4.86	0.55	4.90
Terzan 10	4.42 ¹	-1.89 ¹	-1.00	-6.35	1.55	5.06

¹ Coordinates of Terzan 10 were taken from the 2003 version of Harris (1996) catalog, after analysis of astrometry of VVV images showed that the coordinates provided in the 2010 edition were clearly off.

TABLE 2
SUMMARY OF THE VVV OBSERVATIONS USED.

Cluster	VVV field ID	Filter	Exp.Time ¹	Epochs ²
2MASS-GC02	b326	K_s	8	43 (1-11-21-10)
		H	8	1 (1-0-0-0)
		J	24	1 (1-0-0-0)
		Y	20	2 (1-1-0-0)
		Z	20	2 (1-1-0-0)
Terzan 10	b308	K_s	8	101 (3-7-80-11)
		H	8	1 (1-0-0-0)
		J	24	1 (1-0-0-0)
		Y	20	1 (1-0-0-0)
		Z	20	1 (1-0-0-0)

¹ Effective exposure time, in seconds

² Number of epochs the cluster was observed, with the number of epochs per year from 2010 to 2013 in parentheses

TABLE 3
PROPERTIES OF THE VARIABLE CANDIDATES IN 2MASS-GC02 AND IMMEDIATE SURROUNDINGS.

ID ¹	R.A.(J2000) h:m:s	Dec.(J2000) d:m:s	d^2 arcmin	Period days	A_{K_s}	$\langle K_s \rangle$	$Z - K_s^3$	$Y - K_s^3$	$J - K_s^3$	$H - K_s^3$	Type
NV1	18:09:35.98	-20:47:11.6	0.47	0.700046	0.320	14.566	...	4.313	2.699	0.956	RRab
NV2	18:09:34.22	-20:46:56.1	0.57	0.651668	0.232	14.754	2.881	0.997	RRab
NV3	18:09:33.77	-20:46:29.4	0.68	0.570430	0.266	15.040	3.199	1.094	RRab
NV4	18:09:38.59	-20:46:04.9	0.81	0.623735	0.233	15.301	4.573	1.488	RRab
NV5	18:09:38.86	-20:47:26.4	0.90	0.603298	0.312	14.950	3.257	1.089	RRab
NV6	18:09:33.00	-20:47:07.7	0.91	0.551331	0.386	14.943	2.941	0.989	RRab
NV7	18:09:29.99	-20:45:48.2	1.78	0.569916	0.294	15.453	3.736	1.337	RRab
NV8	18:09:37.70	-20:48:37.5	1.91	0.580325	0.269	14.817	2.867	0.969	RRab
NV9	18:09:45.01	-20:46:09.1	2.07	0.608760	0.256	15.079	3.659	1.218	RRab
NV10	18:09:29.23	-20:48:10.9	2.23	0.489329	0.312	15.217	3.395	1.217	RRab

NOTE. — Table 3 is published in its entirety in the electronic edition of the *Astronomical Journal*. A portion is shown here for guidance regarding its form and content.

¹ Asterisk means that the physical parameters of the star should be considered with caution, since the light curve is not well defined yet.

² Distance to the cluster center

³ Colors measured from single-epoch measurements in Z, Y, J , and H (see Section 4.3 for further explanation).

TABLE 4
SELECTIVE-TO-TOTAL EXTINCTION RATIOS TOWARDS THE STUDIED GCs

	2MASS-GC02	Terzan 10	Nishiyama09	Cardelli89
$A_{K_s}/E(H - K_s)$	$1.27 \pm 0.18 \pm 0.23$	$1.29 \pm 0.23 \pm 0.3$	1.61 ± 0.04	1.87
$A_{K_s}/E(J - K_s)$	$0.40 \pm 0.08 \pm 0.13$	$0.47 \pm 0.05^{+0.03}_{+0.02}$	0.528 ± 0.015	0.72
$A_{K_s}/E(Y - K_s)$...	$0.23 \pm 0.02^{+0.10}_{+0.01}$...	0.43
$A_{K_s}/E(Z - K_s)$...	$0.15 \pm 0.02^{+0.01}_{+0.07}$...	0.31

TABLE 5
DISTANCES AND EXTINCTIONS TO THE STUDIED CLUSTERS

	$R_{\odot, \text{Harris96}}$ (kpc)	$R_{GC, \text{Harris96}}^1$ (kpc)	$E(B - V)_{\text{Harris96}}$	$R_{\odot, \text{derived}}$ (kpc)	$R_{GC, \text{derived}}^1$ (kpc)	$E(J - K_s)_{\text{derived}}$
2MASS-GC02	4.9	-3.6	5.16	$7.1 \pm 0.5 \pm 0.9$	$-1.8 \pm 0.3 \pm 0.6$	3.1
Terzan 10	5.8	-2.6	2.40	$10.3 \pm 0.2 \pm 0.2$	$+2.1 \pm 0.2 \pm 0.2$	0.86

¹ The minus sign indicates location on the near side of the bulge, and the plus sign indicates location on the far side of the bulge. Distances obtained assuming a Galactocentric distance for the Sun of 8.3 kpc (Gillessen et al. 2009; Dékány et al. 2013)

TABLE 6
PROPERTIES OF THE VARIABLE CANDIDATES IN TERZAN 10 AND IMMEDIATE SURROUNDINGS.

ID ¹	R.A.(J2000) h:m:s	Dec.(J2000) d:m:s	d^2 arcmin	Period days	A_{K_s}	$\langle K_s \rangle$	$Z - K_s^3$	$Y - K_s^3$	$J - K_s^3$	$H - K_s^3$	Type
NV1	18:02:58.87	-26:03:35.2	0.53	3.8798	0.402	14.072	2.784	1.942	1.136	0.377	Ecl
NV2	18:02:59.48	-26:04:22.5	0.6	0.730516	0.364	14.608	2.789	1.916	1.068	0.364	RRab
NV3	18:02:54.05	-26:03:46.9	0.78	0.701719	0.323	14.759	3.073	2.092	1.186	0.426	RRab
NV4	18:03:00.19	-26:05:05.8	1.26	0.684468	0.238	14.545	2.241	1.593	0.84	0.305	Ecl
NV5	18:02:57.14	-26:02:43.9	1.27	0.688512	0.294	14.889	4.023	2.695	1.43	0.481	RRab
NV6	18:02:56.90	-26:05:19.6	1.33	0.582339	0.322	14.875	2.97	2.105	1.03	0.384	RRab
NV7	18:02:53.23	-26:05:12.7	1.53	0.715284	0.33	14.711	2.992	2.068	1.016	0.328	RRab
NV8	18:03:03.84	-26:03:13.4	1.64	1.06527	0.295	16.779	2.674	...	0.957	0.149	...
NV9	18:02:51.23	-26:05:14.8	1.87	0.193833	0.259	16.091	2.54	1.82	0.989	0.277	...
NV10	18:03:04.64	-26:05:15.4	2.05	0.211256	0.41	16.203	2.038	1.376	0.816	0.267	...

NOTE. — Table 6 is published in its entirety in the electronic edition of the *Astronomical Journal*. A portion is shown here for guidance regarding its form and content.

¹ Asterisk means that the physical parameters of the star should be considered with caution, since the light curve is not well defined yet.

² Distance to the cluster center

³ Colors measured from single-epoch measurements in Z, Y, J , and H (see Section 5.3 for further explanation).

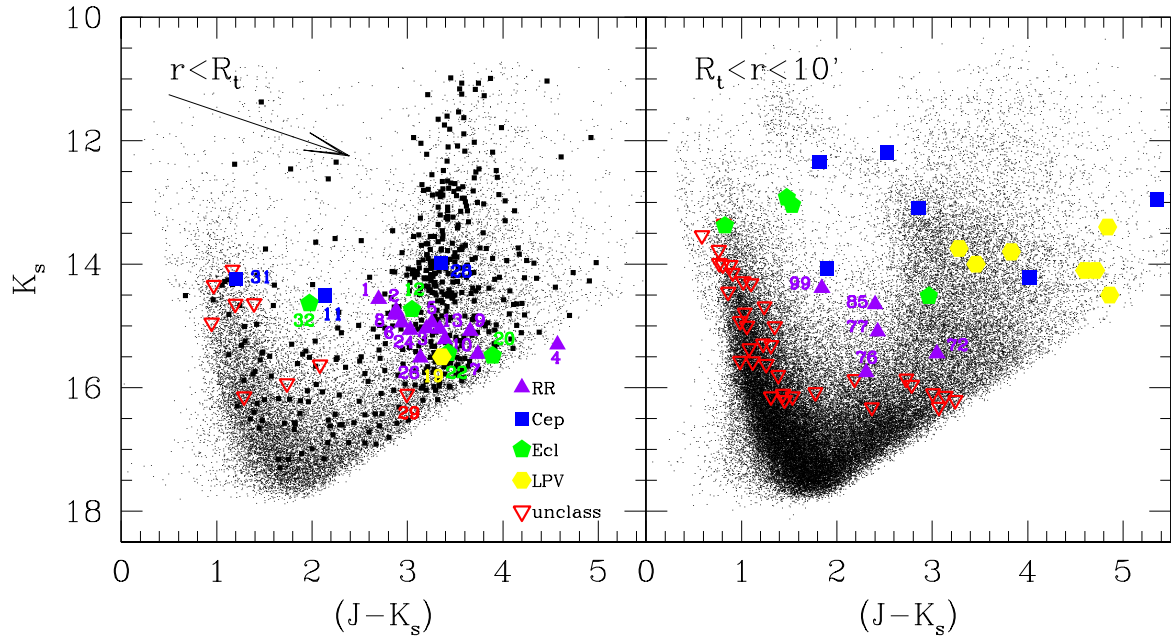


FIG. 1.— $J - K_s$ vs. K_s CMDs of 2MASS-GC02, out to its tidal radius $r_t = 4.9'$ (left), and of its surrounding region (right). The arrow shows the reddening vector according to Nishiyama et al. (2009). In the left panel we have plotted with bigger solid squares the objects out to the cluster's half-light radius, $r_h = 0.55'$. We have also overplotted the positions of RR Lyrae as solid magenta triangles, Cepheids as solid blue squares, eclipsing binaries as solid green pentagons, LPVs as solid yellow hexagons, and unclassified variable candidates as red open triangles. See the electronic edition of the Journal for a color version of this figure*.

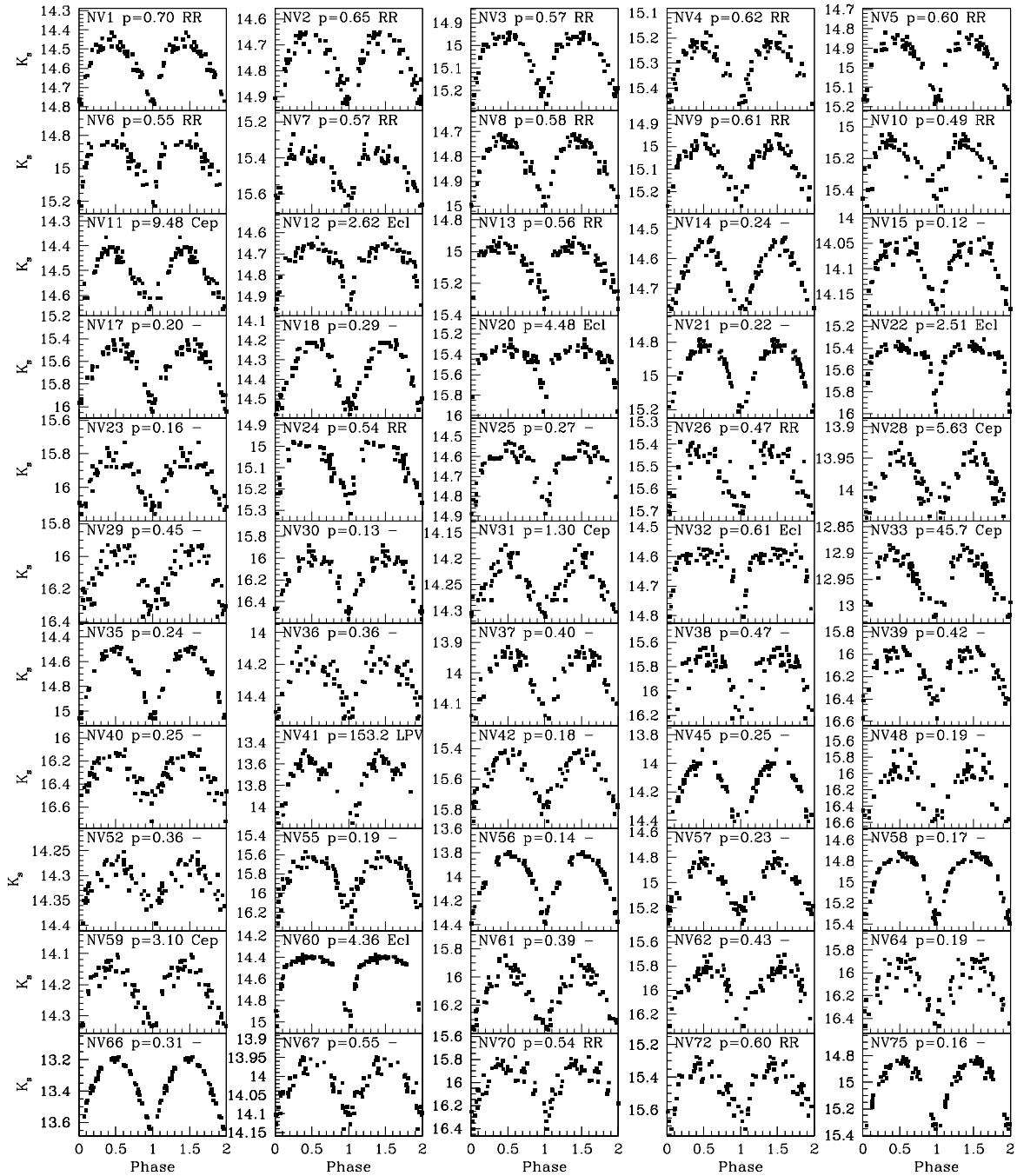
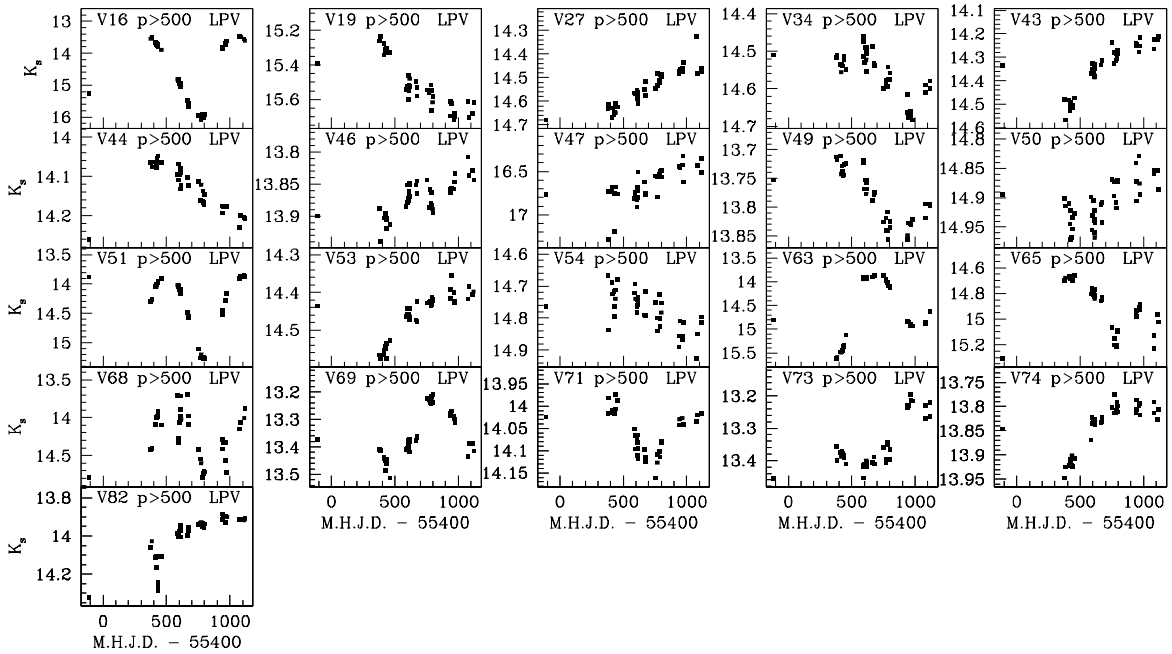
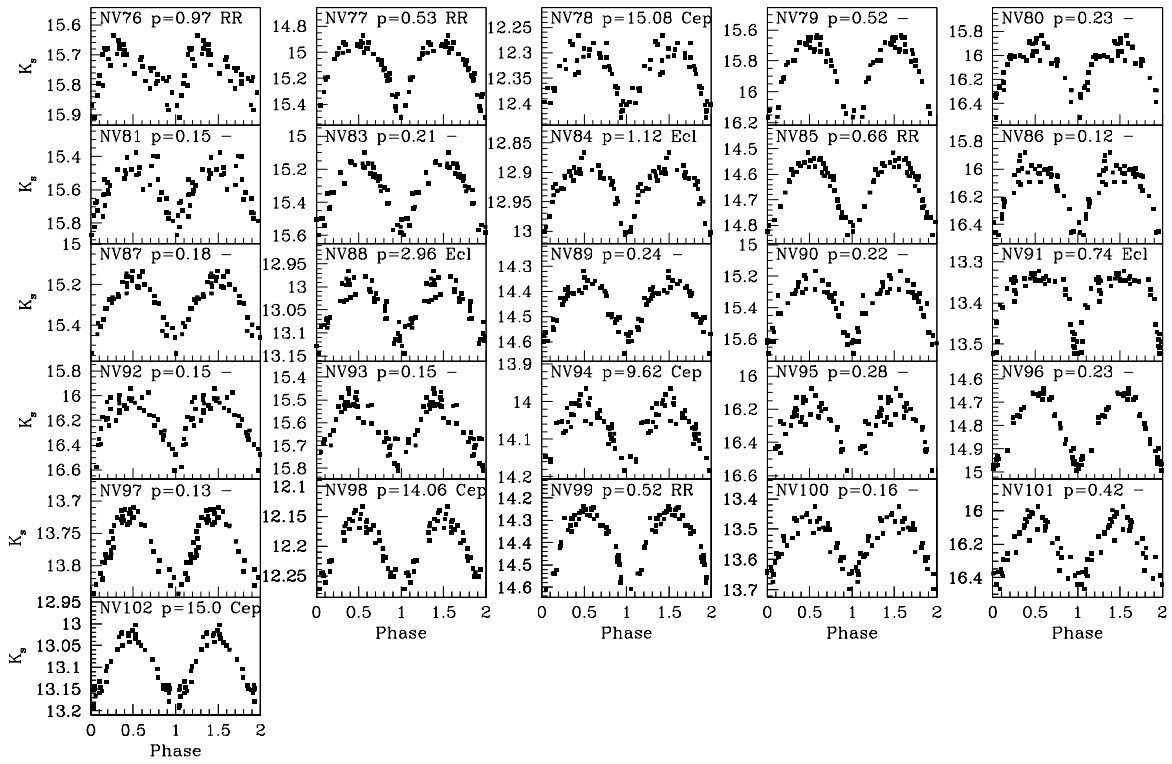


FIG. 2.— Phase-folded light curves of the variable candidates in 2MASS-GC02 and surroundings. The ID, the (rounded) period in days, and the variable type (where available), are indicated at the top of each panel. Light curves for the LPV candidates with periods longer than 500 days are not phase-folded. Supplemental data of this figure* is available in the online journal.



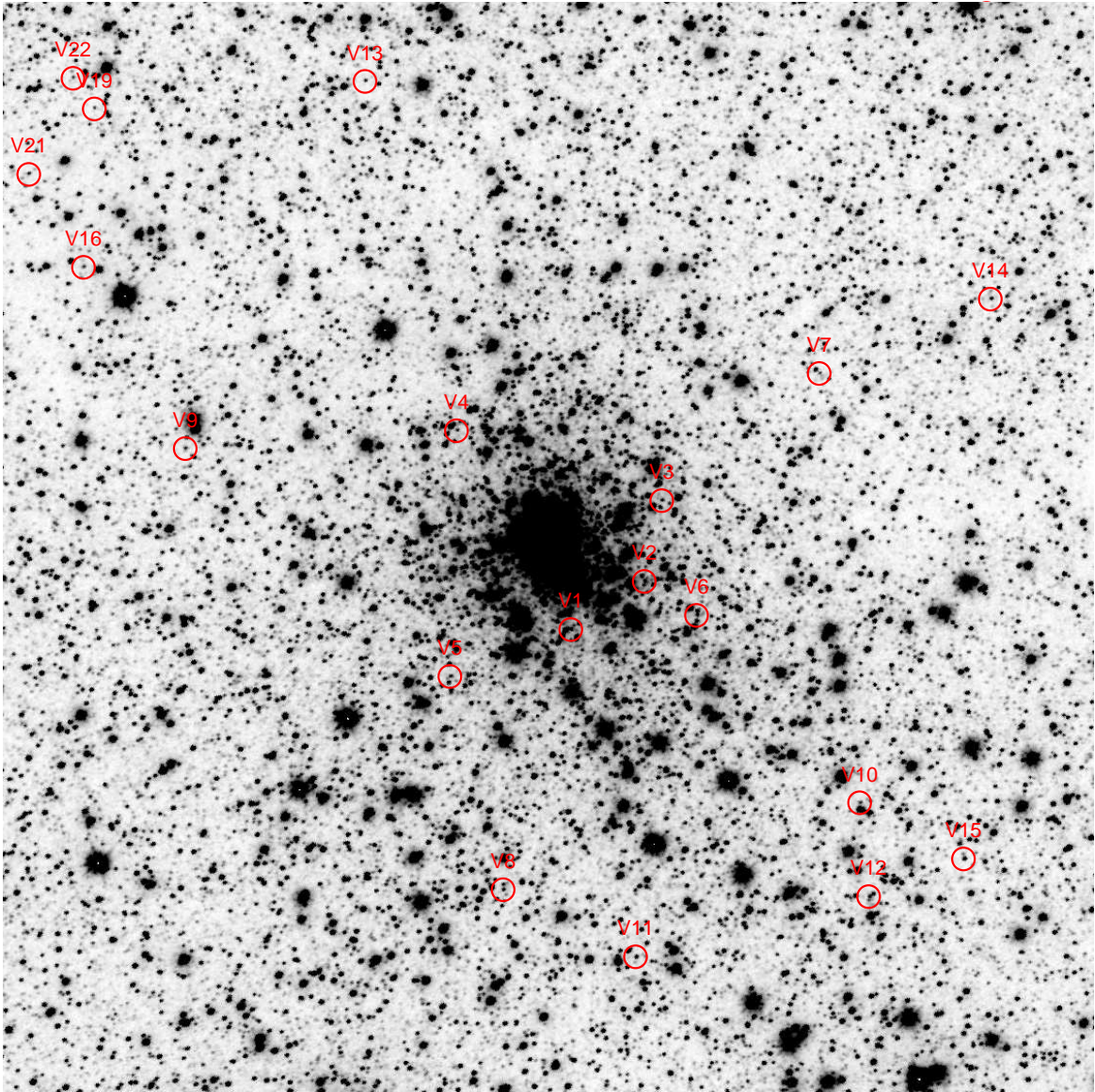


FIG. 3.— K_s -band finding charts for the variables found in 2MASS-GC02 and surroundings. North is up, east is right. The field of view is $6' \times 6'$, and includes most of the RR Lyrae in the cluster. A finding chart with all the variables found (NV1 to NV102) is provided additionally only in the electronic edition.

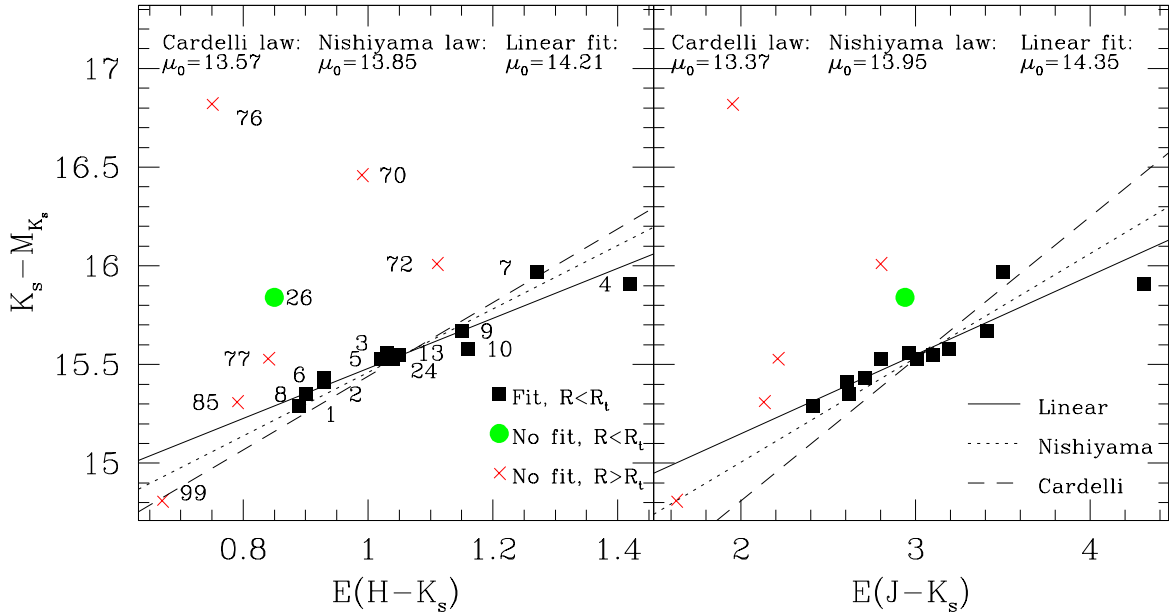


FIG. 4.— Apparent distance modulus vs. color excess diagrams for the RR Lyrae in 2MASS-GC02 and surroundings. A linear fit (solid line) to the cluster RRab variables will give the extinction law (slope of the fit) and the absolute distance modulus (zero-point of the fit) of the cluster. Black squares are the cluster RRab candidates used in the fit, green circles are RRab candidates inside the tidal radius not used in the fit because of their high residuals, and red crosses are RR Lyrae in the surrounding field. As a comparison, we have also plotted the fit using the Cardelli et al. (1989) extinction law (dashed line), and the Nishiyama et al. (2009) extinction law (dotted line).

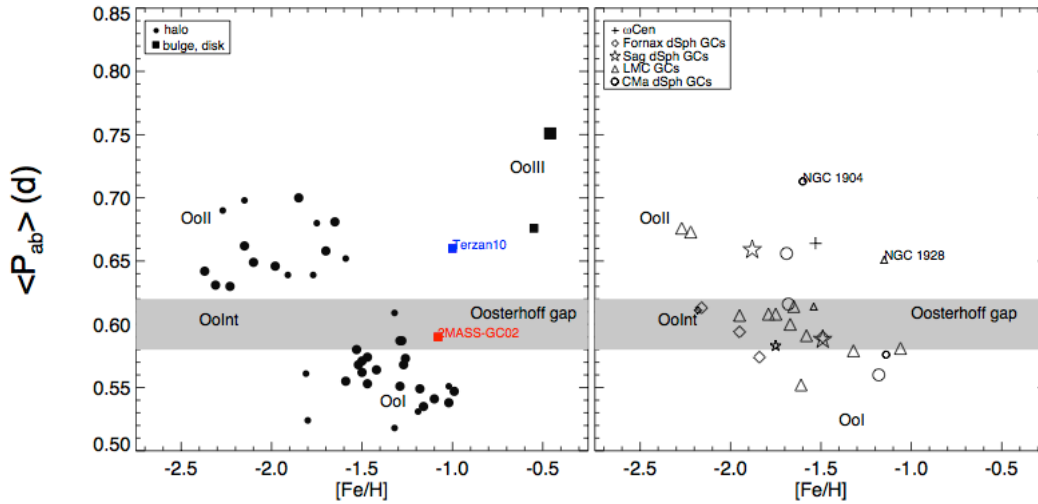


FIG. 5.— Distribution of Galactic GCs (left) and stellar populations associated with neighboring dwarf galaxies (right) in the average ab-type RR Lyrae period (P_{ab}) vs. $[Fe/H]$ plane, updated from Figure 5 in (Catelan 2009a). Smaller symbols indicate that an object contains between 5 and 10 RRab's, while bigger symbols indicate more than 10 RRab's. Locations of 2MASS-GC02 and Terzan 10 have been plotted with different colors, to highlight the unusual positions of both studied GCs in the general Galactic GCs distribution.

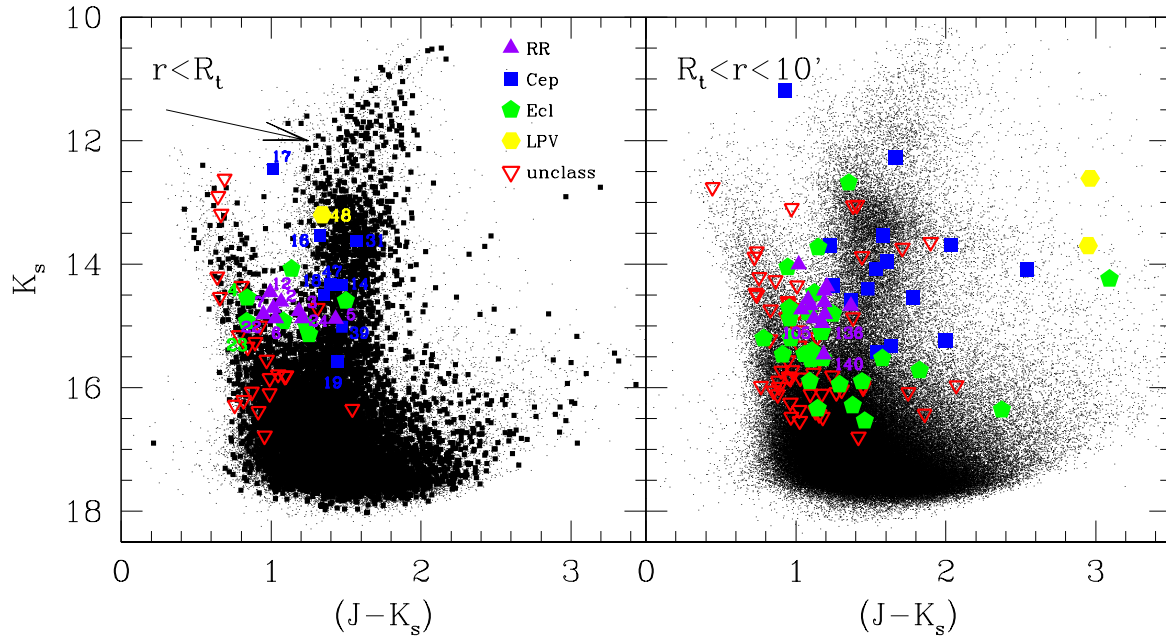


FIG. 6.— As in Figure 1, but for Terzan 10 and its surroundings. In the left panel we have plotted with bigger solid squares the objects out to the cluster's half-light radius, $r_h = 1.55'$.

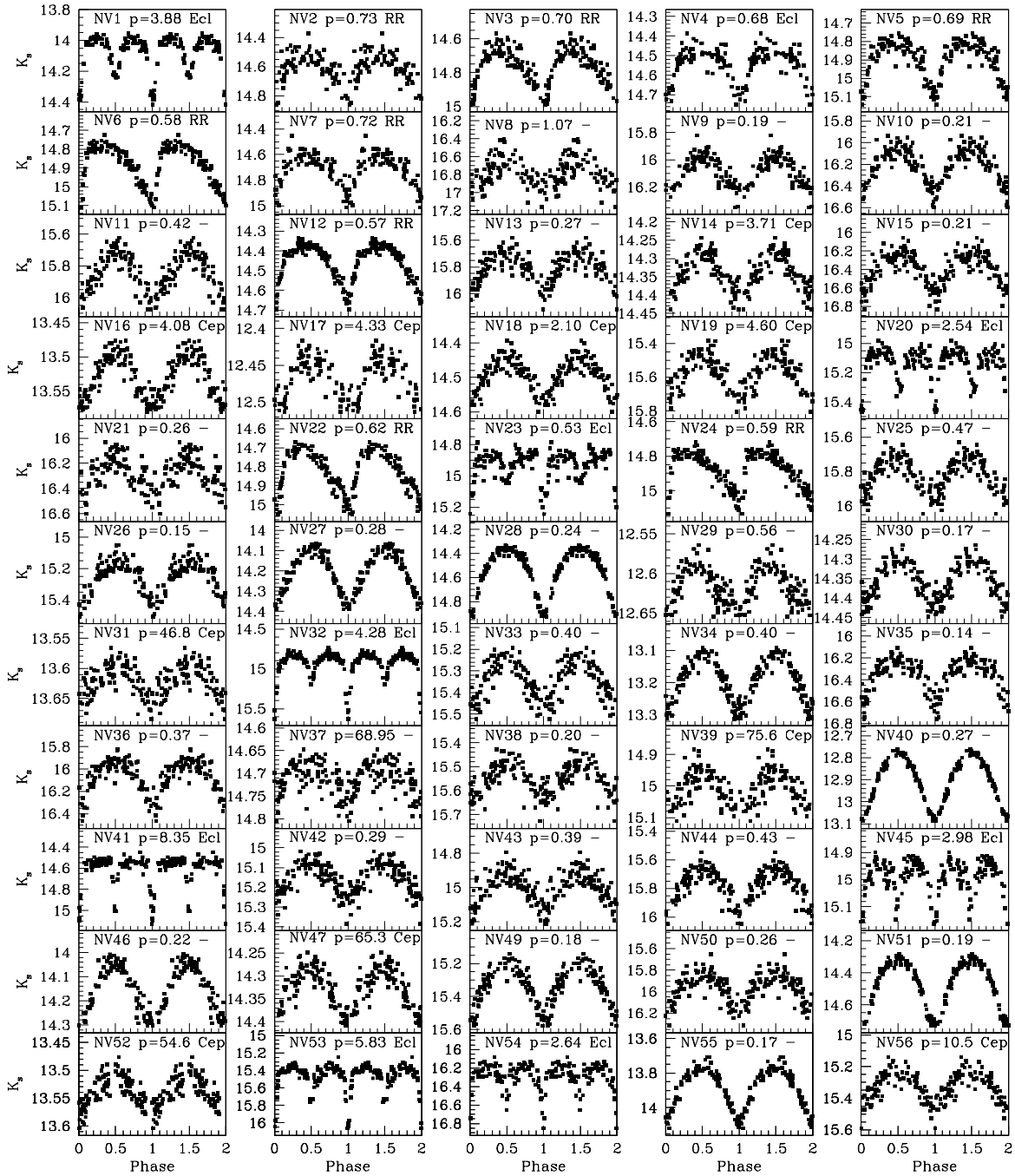
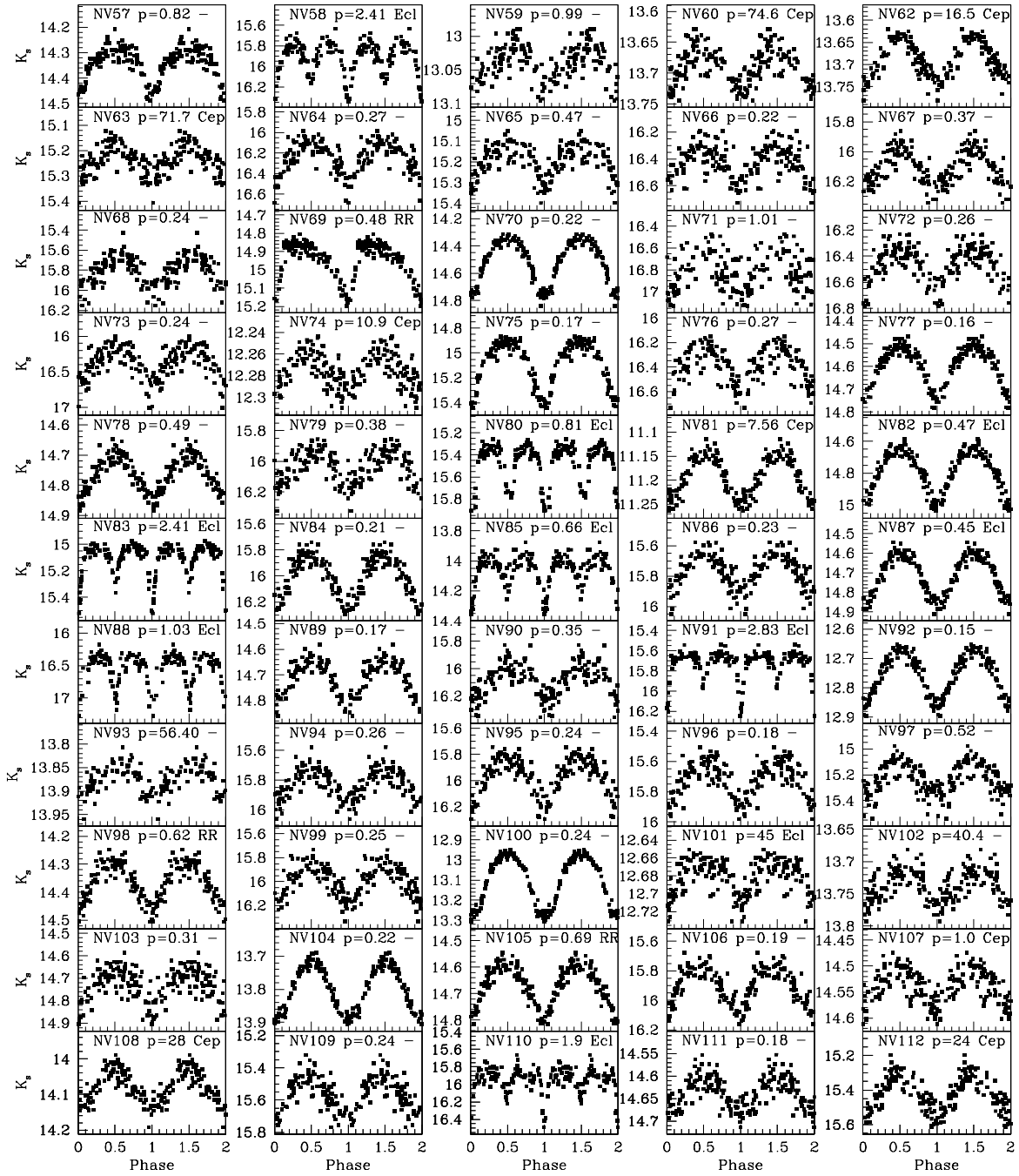
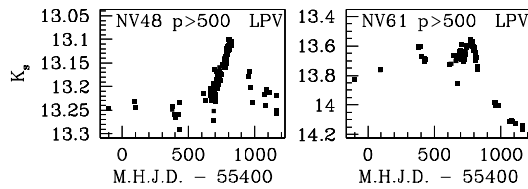
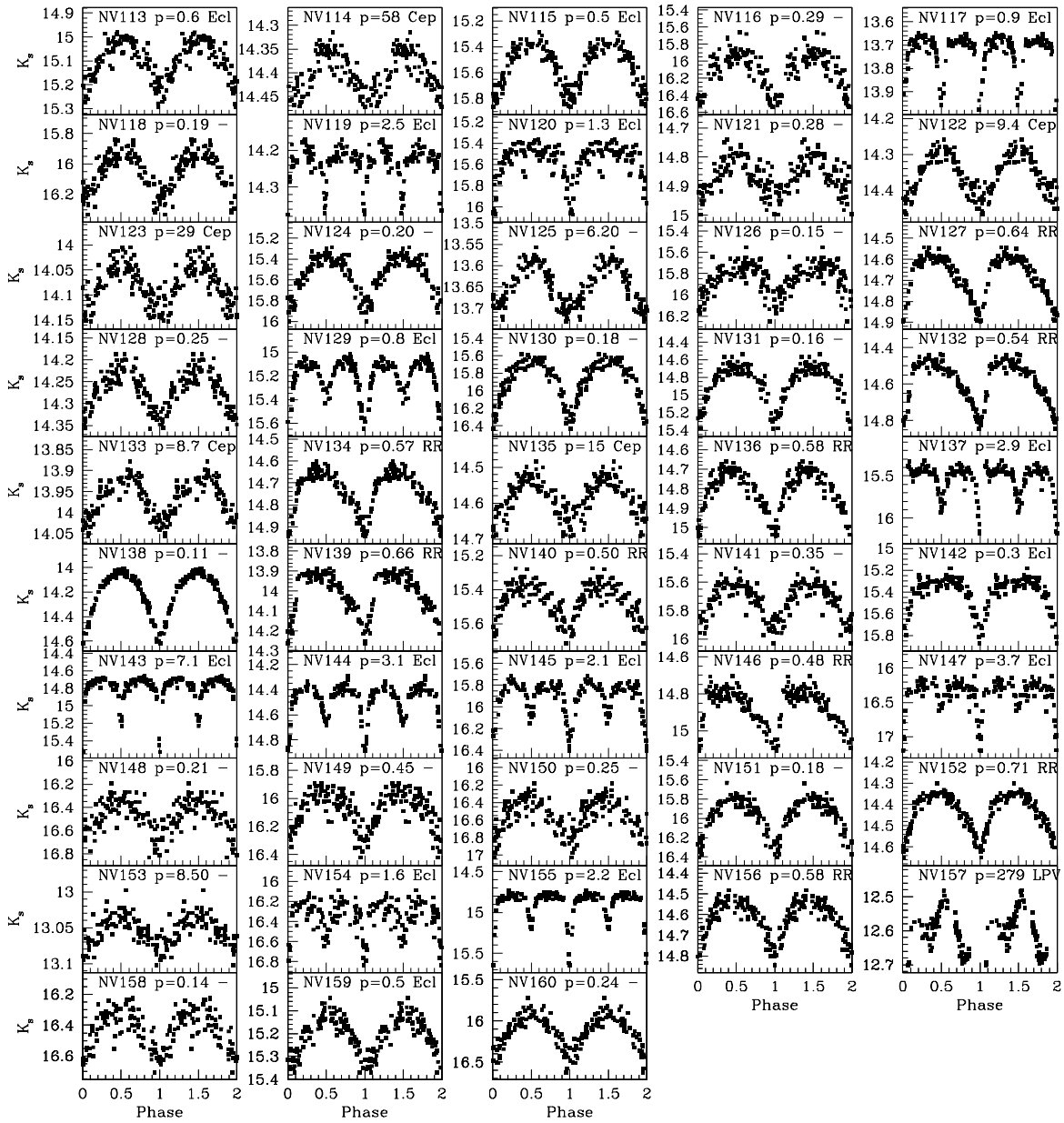


FIG. 7.— As in Figure 2, but for Terzan 10 and its surroundings. Supplemental data of this figure is available in the online journal.





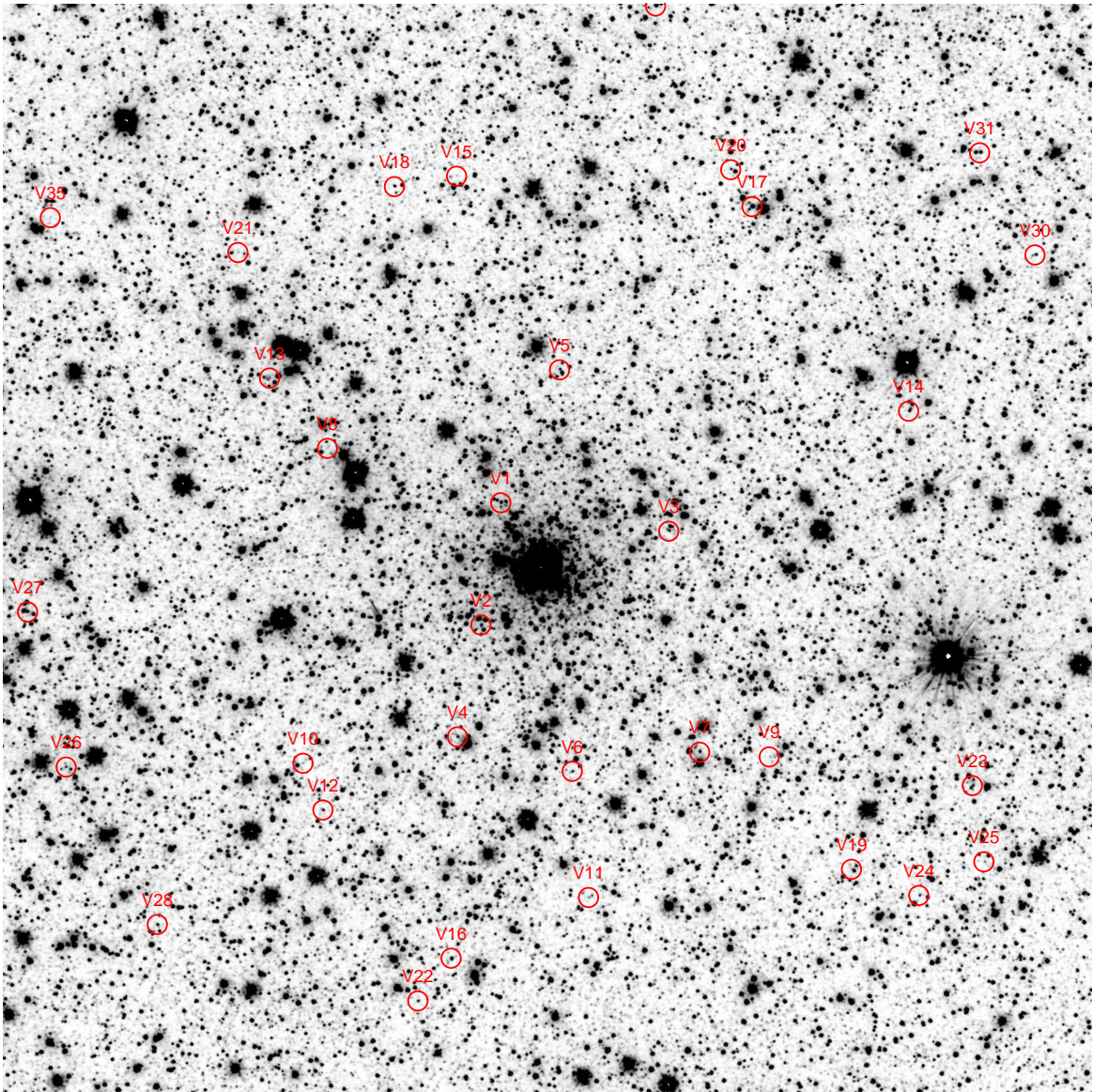


FIG. 8.— As in Figure 3, but for Terzan 10.

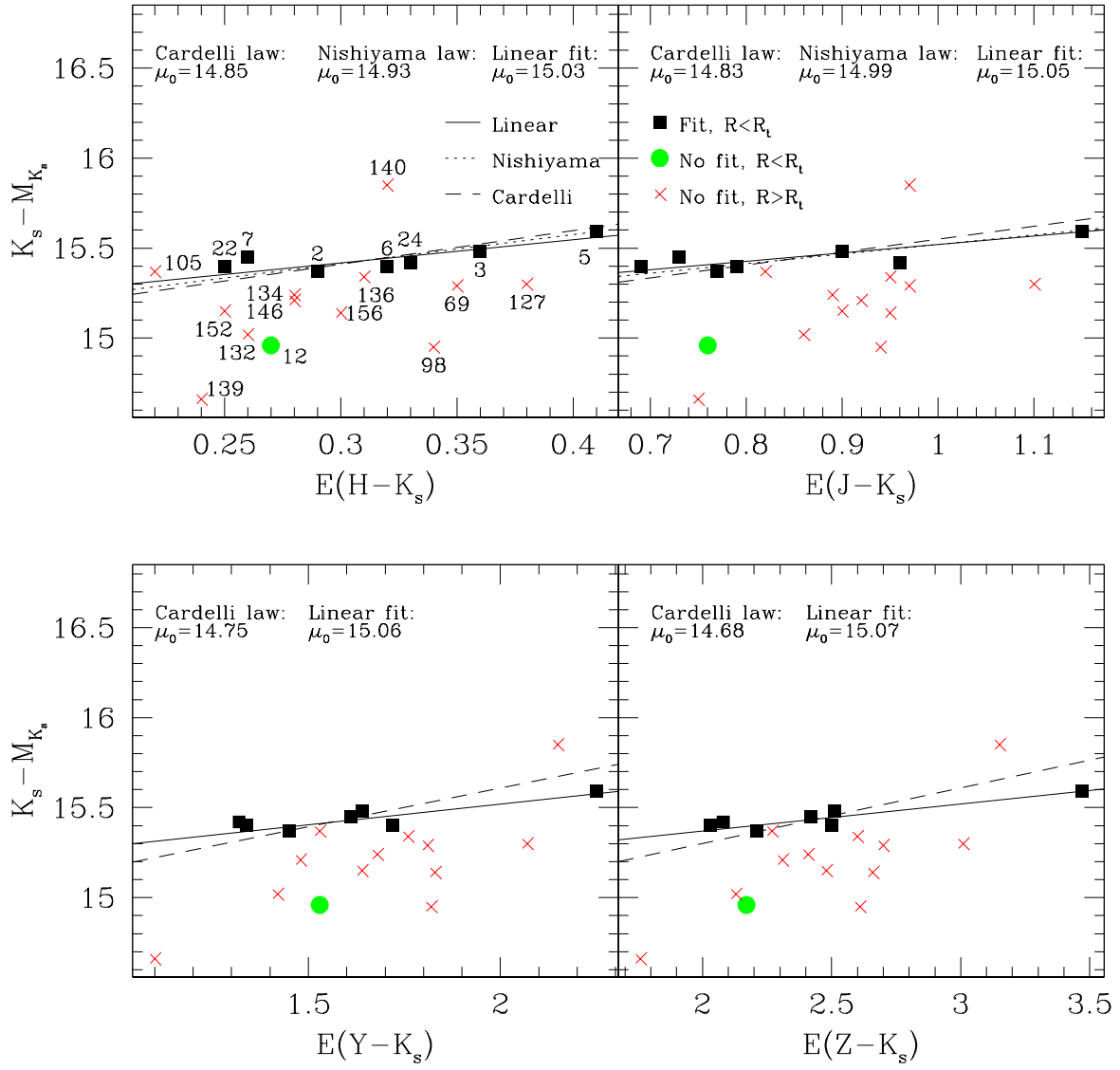


FIG. 9.— As in Figure 4, but for Terzan 10.